Spectrochimica Acta Part A 92 (2012) 365–376

Contents lists available at SciVerse ScienceDirect

Spectrochimica Acta Part A: Molecular and Biomolecular Spectroscopy

journal homepage: www.elsevier.com/locate/saa

The spectroscopic (FT-IR, FT-Raman, UV) and first order hyperpolarizability, HOMO and LUMO analysis of 3-aminobenzophenone by density functional method

M. Karabacak[a], M. Kurt[b], M. Cinar[a], S. Ayyappan[c,d], S. Sudha[e], N. Sundaraganesan[e,*]

[a] Department of Physics, Afyon Kocatepe University, 03040 Afyonkarahisar, Turkey
[b] Department of Physics, Ahi Evran University, 40100 Kırşehir, Turkey
[c] Government College of Technology, Coimbatore 641013, India
[d] Research and Development Centre, Bharathiar University, Coimbatore 641046, India
[e] Department of Physics (Engg.), Annamalai University, Annamalai Nagar, Chidambaram 608002, Tamil Nadu, India

ARTICLE INFO

Article history:
Received 4 October 2011
Received in revised form 13 February 2012
Accepted 17 February 2012

Keywords:
DFT
Vibrational spectra
UV–vis analysis
First order hyperpolarizability
HOMO–LUMO
3-Aminobenzophenone

ABSTRACT

In this work, experimental and theoretical study on the molecular structure and the vibrational spectra of 3-aminobenzophenone (3-ABP) is presented. The vibrational frequencies of the title compound were obtained theoretically by DFT/B3LYP calculations employing the standard 6-311++G(d,p) basis set for optimized geometry and were compared with Fourier transform infrared spectrum (FTIR) in the region of 400–4000 cm^{-1} and with Fourier Transform Raman spectrum in the region of 50–4000 cm^{-1}. Complete vibrational assignments, analysis and correlation of the fundamental modes for the title compound were carried out. The vibrational harmonic frequencies were scaled using scale factor, yielding a good agreement between the experimentally recorded and the theoretically calculated values.

1. Introduction

Benzophenone and its amino-derivatives are used in industry as additives in polymerization mixtures as photo-initiators of polymerization. Benzophenone derivatives, a class of organic materials, are attractive for their large second harmonic generation (SHG) efficiencies and excellent blue light transmittance [1]. A number of benzophenone derivatives show significantly high SHG conversion efficiency. From the past investigations on these molecular systems, it is found that these molecules show high SHG efficiency when p-electron acceptor group is substituted on the benzoyl (Ph—CO—) group rather than on the phenyl group. On the other hand, by placing an electron donor group on each phenyl ring one can substantially enhance the frequency conversion efficiency of these benzophenone derivatives. It is also realized in these molecules that the substitution of weak electron donors such as NH_2, Cl, Br, CH_3 and F groups on phenyl ring results in noncentrosymmetric structures and have been suggested as the best electron donor groups for designing NLO chromophores, considering the transparency and SHG efficiency. Therefore, benzophenone derivatives have been attractive due to their high non linearity as well as for their transparency, and the cross-conjugated path in these molecular systems appears as a powerful electronic system for the molecular engineering of efficient SHG materials.

Both cyclic and acyclic derivatives of 2-aminobenzophenone possess useful pharmacological properties (antithrombotic and psychotropic activities, etc.) [2,3]. The 2-aminobenzophenones have drawn much attention due to the fact that they are among the important starting materials for the synthesis of a wide variety of heterocyclic systems [4–8]. In particular, it has been reported that 2-aminobenzophenones can be used as intermediates for the synthesis of numerous CNS drugs of the 1,4-benzodiazepine class [9].

Recently, Duan et al. [10] investigated the intramolecular charge transfer and solvent effect of dimethylaminobenzophenone by TD-DFT study. Cheng et al. [11] studied the absorption spectra and photoreactivity of p-aminobenzophenone by TD-DFT method. Sett et al. [12] have investigated the DFT calculation and Raman excitation studies of benzophenone molecule. Tsonkov and Bistra [13] studied the vibrational spectra and structure of benzophenone in solid state and in solution. Hong et al. [14] have reported the molecular structure and vibrational spectra of benzophenone hydrazone by density functional theory. Literature survey reveals that to the best of our knowledge, theoretical calculations using DFT method

* Corresponding author. Tel.: +91 9442068405.
E-mail address: sundaraganesan_n2003@yahoo.co.in (N. Sundaraganesan).

1386-1425/$ – see front matter © 2012 Elsevier B.V. All rights reserved.
doi:10.1016/j.saa.2012.02.067

with 6-311++G(d,p) basis set of 3-ABP have not been reported so far. It is, therefore thought worthwhile to make a comprehensive vibrational analysis using both experimentally observed IR and Raman wavenumbers and theoretically calculated vibrational spectra.

In our present study, the optimized structural parameters and the vibrational characteristics of 3-ABP were investigated using DFT/B3LYP calculations. The calculated vibrational frequencies have been compared with the experimentally recorded values and complete vibrational assignment, analysis and correlation of the fundamental modes of this compound have been performed. Density functional theory (DFT) approaches, especially those using hybrid functional, have evolved to be a powerful and very reliable tool, being routinely used for the determination of various molecular properties. These calculations combined with experimental spectral techniques provide a lot of information that is useful for understanding the molecular structures and the vibrational spectra of various types of organic compounds.

2. Experimental

The 3-ABP compound was purchased from Sigma–Aldrich Chemical Company with a stated purity of 97% and was used as such without further purification. The FT-IR spectrum of KBr disc of the sample was recorded on a Perkin Elmer FT-IR BX spectrometer in the 4000–400 cm^{-1} range. The FT-Raman spectrum of the samples was recorded using the 1064 nm line of a Nd:YAG laser for excitation in the region 4000–50 cm^{-1} on a Bruker model FRA 106/S FT-Raman spectrometer. The detector was a liquid-nitrogen cooled Ge detector. The ultraviolet (UV) absorption spectrum of the compound was examined in the range 200–800 nm using Shimadzu UV-1700 PC, UV–vis recording spectrophotometer. The UV pattern is taken from a 10^{-5} molar solution of 3-ABP, solved in ethanol.

3. Computational details

The combination of spectroscopic methods with DFT calculations are powerful tools for understanding the fundamental vibrational properties and the electronic structure of the compounds. In order to provide information with regard to the structural characteristics and the normal vibrational modes of 3-ABP, the DFT-B3LYP correlation functional calculations have been carried out. The calculations of geometrical parameters in the ground state were performed using the Gaussian 03 [15] program. The input geometry of 3-ABP molecule has been first optimized without any constraint in the potential energy surfaces at DFT/B3LYP level adopting the standard 6-311++G(d,p) basis set for C, N and H atoms. Many studies [16–18] have shown that the DFT-B3LYP method in combination with the 6-31++G(d, p) and 6-311++G(d, p) basis sets are able to give the accurate energies, molecular structures, infrared and Raman vibrational frequencies. The resultant-optimized geometry has been used as input for vibrational frequency calculations at DFT/B3LYP level to characterize all stationary points as minima. To define the nature of the acquired stationary points and to account for the zero point vibrational energy (ZPVE) corrections, harmonic vibrational frequencies were computed at the same levels of theory. The polarization functions have been added for the better treatment of amino group. DFT method, including local or non-local functionals, yields molecular force fields and vibrational wavenumbers are in excellent agreement with experiment. Among the numerous available DFT methods, we have selected the B3-LYP [19–21] method, which combines the Becke's three-parameter exchange functional (B3) [19] with the Lee, Young and Parr correlation functional (LYP) [20]. The theoretical results have enabled us to make detailed assignments of the experimental IR spectrum of 3-ABP molecule. All results were obtained by using GaussView 3.0 molecular visualization program [22]. The vibrational modes were assigned on the basis of TED analysis using PQS program [23]. The electronic properties such as HOMO and LUMO energies were determined by time-dependent DFT (TD-DFT) approach, while taking solvent effect into account.

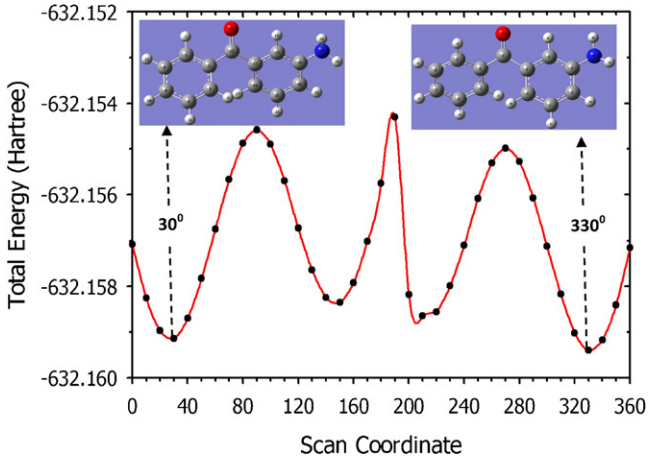

Fig. 1. PES scan for the selected torsional angle D(C15—C13—C12—O23) of freedom.

4. Prediction of Raman intensities

The Raman activities (S_{Ra}) calculated with Gaussian 03 program [15] converted to relative Raman intensities (I_{Ra}) using the following relationship derived from the intensity theory of Raman scattering [24,25].

$$I_i = \frac{f(\nu_0 - \nu_i)^4 S_i}{\nu_i[1 - \exp(-hc\nu_i/kT)]}$$

where, ν_0 is the laser exciting wavenumber in cm^{-1} (in this work, we have used the excitation wavenumber $\nu_0 = 9398.5\ cm^{-1}$, which corresponds to the wavelength of 1064 nm of a Nd:YAG laser), ν_i the vibrational wavenumber of the ith normal mode (cm^{-1}), while S_i is the Raman scattering activity of the normal mode ν_i. f (is a constant equal to 10^{-12}) is a suitably chosen common normalization factor for all peak intensities. h, k, c and T are Planck, Boltzmann constants, speed of light and temperature in Kelvin, respectively. For simulation, the calculated FT-Raman spectrum has been plotted using pure Lorentzian band shape with a bandwidth of full width and half maximum (FWHM) of 10 cm^{-1}.

5. Results and discussion

5.1. Conformational analysis

To find stable conformers, a meticulous conformational analysis was carried out for our title molecule. The full geometry optimization of these structures were performed by B3LYP/6-311++G(d,p) method. The potential energy surface (PES) scan is performed for C=O and amino group using B3LYP/6-311++G(d,p) level of theoretical approximation for our title compound is shown in Fig. 1. The dihedral angles C1—C2—C12—O23, C15—C13—C12—O23 and C15—C18—N24—H25 for 3-ABP is also the relevant coordinate for conformational flexibility within the molecule. During the calculation, the lateral dihedral angle C15—C18—N24—H25 is fixed while the C1—C2—C12—O23 and C15—C13—C12—O23 torsional angles were varied in steps of 5°, 10°, 15°, 20°, ..., 360°. Results showed that low energy domains for the dihedral angle (O23—C12—C13—C15) are located at 30° and 330°

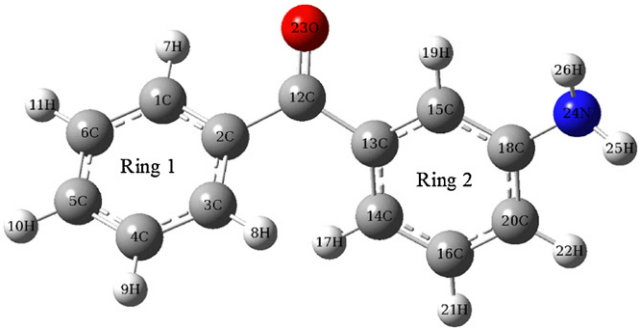

Fig. 2. Molecular structure with atom numbering scheme of 3-ABP.

with −632.1591375 and −632.1593991 Hartree, respectively. In the mean time, the high energy conformer located at 190° with −632.154305 Hartree. The energy difference between the most favorable and unfavorable conformers, which arise from the rotational potential barrier calculated with respect to the selected torsional angle, is calculated as 0.0050941 Hartree (3.1965936 K Cal mol^{-1}).

5.2. Structural analysis

The first task for the computational work is to determine the optimized geometries of the studied molecule. The geometry of the molecule under investigation is considered by possessing C_1 point group symmetry. The 3-ABP is an asymmetric top. The comparative optimized structural parameters such as bond lengths, bond angles and dihedral angles are presented in Table 1 in accordance with atom numbering scheme shown in Fig. 2. The dipole moment, polarizability and first hyperpolarizability are given in Table 2. All the geometries determined belong to a true minimum proven by all real wavenumbers in the vibrational analysis as seen from Table 3. Since the exact crystal structure of the 3-ABP compound is not available till now, the optimized structure can be only compared with other similar system benzophenone [13] for which the crystal structure has been solved. As seen from Table 1, most of the optimized bond lengths are slightly longer than the experimental values and the bond angles are slightly different from the experimental ones, because the molecular states are different during experimental and theoretical processes. Although the differences, calculated geometrical parameters represent a good approximation and they can be used as foundation to calculate the other parameters, such as vibrational frequencies and thermodynamics properties.

The molecular structure is non-planar and the tilting takes place between the two rings is due to steric repulsion between the two rings. The two rings of 3-ABP molecule are not co-planar mainly due to the repulsion between the 8H and 17H hydrogen atoms. This fact is also evident from the dihedral angles, C3—C2—C12—C13 = 33.4°, C2—C12—C13—C14 = 31.0°, C1—C2—C12—C13 = −150.4° and C2—C12—C13—C15 = −152.7° calculated by B3LYP/6-311++G(d,p) method as shown in Table 1. For benzophenone hydrazone molecule, the two benzene rings, each forming a plane with their dihedral angle of 74.4° at B3LYP/6-311+G(d,p) level [13].

The C—C bond connecting the two rings shows a much higher double bond character, where both C2—C12 and C12—C13 bond lengths are 1.501 Å, the rest of the bond lengths range from 1.390 Å to 1.405 Å. This may suggest that 3-ABP is a π electron delocalized system, a highly conjugated molecule, and hence shows small deviation from co-planarity. It seems that the oxygen O23 atom contributes to the delocalization of the π electrons in the system allowing the compound to behave aromatically. Another important thing to notice is that C12—O23 [1.221 Å] bond length is smaller compared to the other bond lengths. This would suggest that the π electrons tend to be mostly localized in the vicinity of the C12—O23 bond. From the above observations, one can confirm that the 3-ABP molecule is highly conjugated and π electron delocalized. The charge transfer takes place between the two benzene rings through the carbonyl group, so it acts as a bridging mode. The C—H bond lengths range from 1.082 to 1.084 Å and the deviation is 0.002 Å. Both the N—H bond lengths are 1.009 Å.

5.3. Vibrational assignments

In order to obtain the spectroscopic signature of the selected compound, we performed a frequency calculation analysis. The maximum number of potentially active observable fundamentals of a non-linear molecule which contains N atoms is equal to (3N-6), apart from three translational and three rotational degrees of freedom. The main focus on the present investigation is the proper assignment of the experimental frequencies to the various vibrational modes of 3-ABP in corroboration with the scaled down calculated harmonic vibrational frequencies at B3LYP level using 6-311++G(d,p) basis set. The molecular conformation obtained from the crystalline structure, as well as the one yielded by geometry optimization, exhibits no special symmetries and hence the molecule belongs to the C_1 point group. As a consequence, all the 72 fundamental vibrations of the free molecule are both IR and Raman active. The atomic displacements corresponding to the different normal modes are identified using GaussView program package [22,26]. The comparative IR and Raman spectra of experimental and calculated (B3LYP) are given in Fig. 3. The observed and calculated frequencies along with their relative intensities, probable assignments and total energy distribution (TED) of 3-ABP are summarized in Table 3.

The normal modes for the comparison of experimental and theoretical results presented in Table 3 were selected basically on two criteria: (i) the modes which are nearly pure modes, where contribution of one internal coordinate to TED is more than 80% and (ii) the modes, which are observed more prominently in the Raman and IR spectra and also show a good intensity in calculations. A dual scaling factor gives better agreement between the calculated and observed wavenumbers, in comparison to uniform scaling factor. In view of these forgoing discussion dual scaling method in which the scaling factors are 0.9927 and 0.9659 for the fingerprint (below 1800 cm^{-1}) and *X–H* stretching (above 1800 cm^{-1}) regions, respectively were used in this study to offset the systematic error caused by neglecting harmonicity and electron density [27]. The scaled calculated frequencies minimize the root-mean square difference between calculated and experimental frequencies for bands with definite identifications.

5.3.1. C—H vibrations

The existence of one or more aromatic rings in a structure is normally readily determined from the C—H and C=C—C ring related vibrations. The C—H stretching occurs above 3000 cm^{-1} and is typically exhibited as a multiplicity of weak to moderate bands, compared with the aliphatic C—H stretch [28]. These vibrations are not found to be affected due to the nature and position of the substituents. In our present work, the C—H stretching vibration of benzophenone ring is observed in FT-IR spectrum at 3203, 3079, 3056, 3027 cm^{-1} and in FT-Raman spectrum at 3200, 3062 cm^{-1}. The similar vibration is calculated in the range 3068–3025 cm^{-1} by B3LYP/6-311++G(d,p) method and it shows good correlation with the experimental data. As indicated by the TED, these modes (mode nos. 3–11) involve more than 90% of contribution suggesting that they are pure stretching modes. All the aromatic C—H stretching

Table 1
The calculated geometric parameters of 3-aminobenzophenone, bond lengths in angstrom (Å) and angles in degrees (°).

Parameters	B3LYP	X-ray[a]	Parameters	B3LYP	X-ray[a]
Bond lengths (Å)			Bond angles (°)		
C1—C2	1.402	1.388	C2—C3—C4	120.3	118.6
C1—C6	1.390	1.402	C2—C3—H8	119.9	
C1—H7	1.083		C4—C3—H8	119.7	
C2—C3	1.401	1.400	C3—C4—C5	120.1	120.3
C2—C12	1.501	1.496	C3—C4—H9	119.8	
C3—C4	1.394	1.408	C5—C4—H9	120.1	
C3—H8	1.083		C4—C5—C6	119.9	120.6
C4—C5	1.394	1.367	C4—C5—H10	120.0	
C4—H9	1.084		C6—C5—H10	120.0	
C5—C6	1.396	1.354	C1—C6—C5	120.0	120.8
C5—H10	1.084		C1—C6—H11	119.9	
C6—H11	1.084		C5—C6—H11	120.0	
H7—O23	2.556		C2—C12—C13	120.1	121.6
C12—C13	1.501		C2—C12—O23	119.7	
C12—O23	1.221		C13—C12—O23	120.2	
C13—C14	1.401		C12—C13—C14	122.4	
C13—C15	1.398		C12—C13—C15	117.6	
C14—C16	1.394		C14—C13—C15	119.9	
C14—H17	1.082		C13—C14—C16	119.2	
C15—C18	1.399		C13—C14—H17	120.6	
C15—H19	1.084		C16—C14—H17	120.2	
C16—C20	1.390		C13—C15—C18	121.0	
C16—H21	1.084		C13—C15—H19	118.5	
C18—C20	1.405		C18—C15—H19	120.5	
C18—N24	1.394		C14—C16—C20	120.9	
H19—O23	2.523		C14—C16—H21	119.8	
C20—H22	1.086		C20—C16—H21	119.3	
N24—H25	1.009		C15—C18—C20	118.5	
N24—H26	1.009		C15—C18—N24	120.8	
Bond angles (°)			C20—C18—N24	120.6	
C2—C1—C6	120.4	119.7	C16—C20—C18	120.5	
C2—C1—H7	118.7		C16—C20—H22	120.0	
C6—C1—H7	120.9		C18—C20—H22	119.5	
C1—C2—C3	119.2		C18—N24—H25	116.3	
C1—C2—C12	118.1		C18—N24—H26	116.1	
C3—C2—C12	122.6	118.2	H25—N24—H26	112.8	
Dihedral angle (°)			Dihedral angle (°)		
C6—C1—C2—C3	−1.4		H10—C5—C6—C1	179.4	
C6—C1—C2—C12	−177.6		H10—C5—C6—H11	−0.1	
H7—C1—C2—C3	178.5		O23—C12—C13—C14	−148.9	
H7—C1—C2—C12	2.3		O23—C12—C13—C15	27.3	
C2—C1—C6—C5	1.4		C12—C13—C14—C16	176.3	
C2—C1—C6—H11	−179.0		C12—C13—C14—H17	−1.8	
H7—C1—C6—C5	−178.5		C15—C13—C14—C16	0.1	
H7—C1—C6—H11	1.1		C15—C13—C14—H17	−178.0	
C1—C2—C3—C4	0.2		C12—C13—C15—C18	−177.6	
C1—C2—C3—H8	−178.4		C12—C13—C15—H19	1.7	
C1—C2—C12—C13	−150.4		C14—C13—C15—C18	−1.2	
C12—C2—C3—C4	176.2		C14—C13—C15—H19	178.0	
C12—C2—C3—H8	−2.4		C13—C14—C16—C20	0.9	
C1—C2—C12—O23	29.5		C13—C14—C16—H21	−179.0	
C3—C2—C12—C13	33.4		H17—C14—C16—C20	179.1	
C3—C2—C12—O23	−146.6		H17—C14—C16—H21	−0.8	
C1—C2—C13—C14	−108.6		C13—C15—C18—C20	1.3	
C1—C2—C13—C15	87.5		C13—C15—C18—N24	178.2	
C3—C2—C13—C14	53.8		H19—C15—C18—C20	−178.0	
C3—C2—C13—C15	−110.0		H19—C15—C18—N24	−1.1	
C2—C12—C13—C14	31.0		C14—C16—C20—C18	−0.9	
C2—C12—C13—C15	−152.7		C14—C16—C20—H22	179.8	
C2—C3—C4—C5	1.0		H21—C16—C20—C18	179.0	
C2—C3—C4—H9	−178.9		H21—C16—C20—H22	−0.3	
H8—C3—C4—C5	179.6		C15—C18—C20—C16	−0.2	
H8—C3—C4—H9	−0.3		C15—C18—C20—H22	179.1	
C3—C4—C5—C6	−1.0		N24—C18—C20—C16	−177.1	
C3—C4—C5—H10	179.4		N24—C18—C20—H22	2.2	
H9—C4—C5—C6	179.0		C15—C18—N24—H25	158.2	
H9—C4—C5—H10	−0.7		C15—C18—N24—H26	21.9	
C4—C5—C6—C1	−0.2		C20—C18—N24—H25	−25.0	
C4—C5—C6—H11	−179.8		C20—C18—N24—H26	−161.3	

[a]Taken from Ref. [13].

Table 2
The electric dipole moment μ (D), polarizability and first order hyperpolarizability of 3-aminobenzophenone.

	B3LYP/6-311++G(d,p)			B3LYP/6-311++G(d,p)	
	a.u.	esu ($\times 10^{-24}$)		a.u.	esu ($\times 10^{-33}$)
α_{xx}	228.09141	33.80315	β_{xxx}	158.03415	1365.30445
α_{xy}	7.04660	1.04431	β_{xxy}	140.26495	1211.79101
α_{yy}	105.92802	15.69853	β_{xyy}	57.70893	498.56478
α_{xz}	−27.39356	−4.05973	β_{yyy}	5.47475	47.29802
α_{yz}	−5.93235	−0.87917	β_{xxz}	−141.47421	−1222.23813
α_{zz}	168.34998	24.94947	β_{xyz}	18.12707	156.60522
α_{tot}	167.45647	24.81705	β_{yyz}	28.29163	244.41985
$\Delta\alpha$	117.04905	17.34667	β_{xzz}	274.97821	2375.61922
μ_x	1.0156		β_{yzz}	−42.78513	−369.63356
μ_y	−2.9674		β_{zzz}	−189.67976	−1638.70033
μ_z	1.4336		β_{tot}	648.682182	5604.15997
μ	3.4485				

bands are found to be weak and this is due to the decrease of dipole moment caused by the reduction of negative charge on the carbon atom. This reduction occurs because of the electron withdrawal on the carbon atom by the substituent due to the decrease of inductive effect, which in turn is caused by the increased chain length of the substituent [29].

The aromatic C—H in-plane bending vibrations of benzene and its derivatives are observed in the region 1300–1000 cm^{-1} [30]. The bands are sharp but weak to medium intensity. In our present work, the calculated vibrations (mode nos. 23–35) by DFT method are predicted in the range 1329–1031 cm^{-1}. These vibrations are assigned to C—H in-plane bending vibration of aromatic ring, which

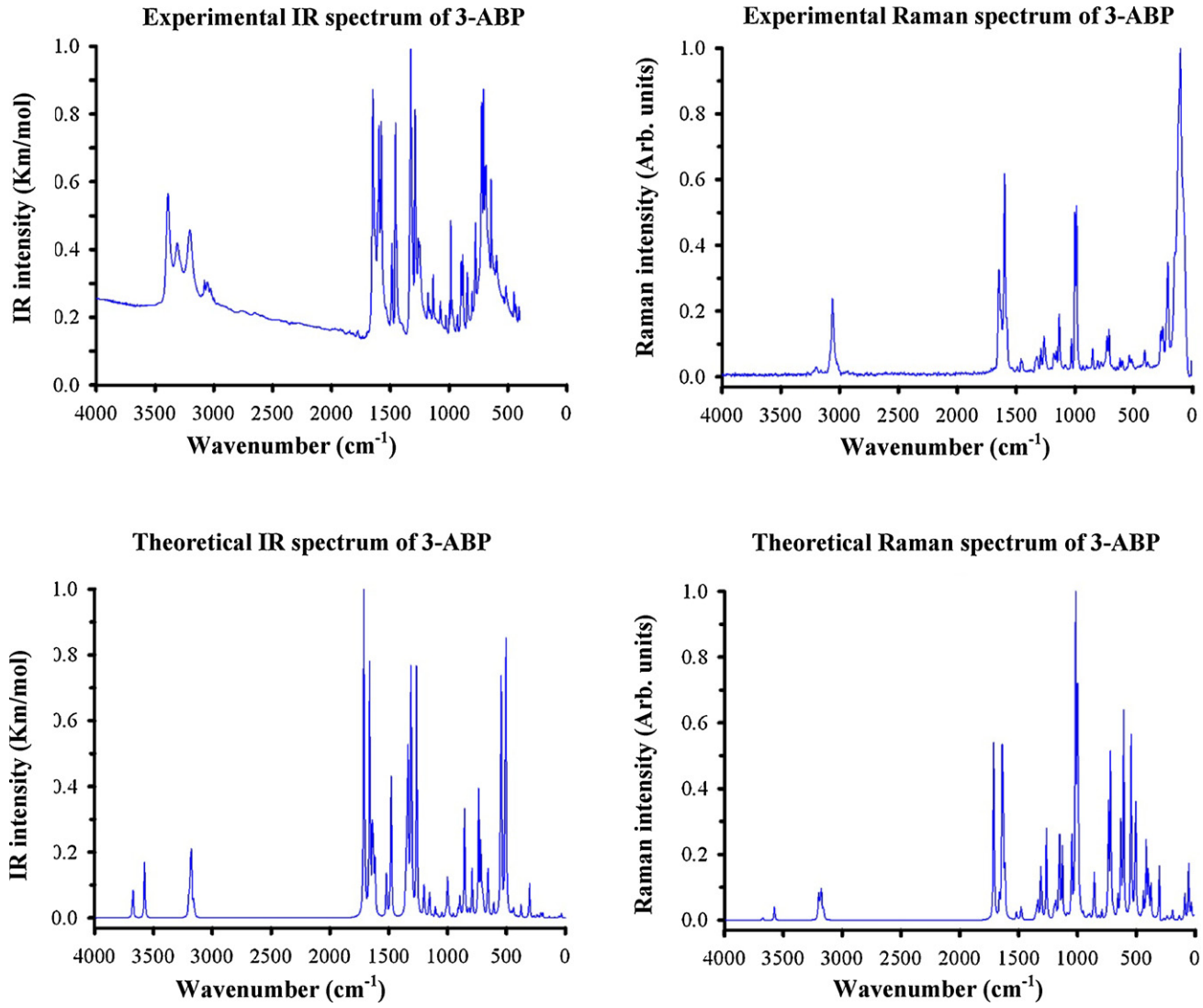

Fig. 3. Experimental and theoretical IR and Raman spectra of 3-ABP.

Table 3
Comparison of the calculated and experimental vibrational spectra and proposed assignments of 3-aminobenzophenone.

Mode nos.	Experimental wavenumbers (cm^{-1})			Theoretical wavenumbers (cm^{-1}) B3LYP/6-311++G(d,p)				Vibrational assignments with TED (≥10%)
	FT-IR	FT-Raman	Unscaled	Scaled	I_{IR}[a]	SA_{Ra}[b]	I_{Ra}[c]	
1	3389s		3674	3520	19.06	61.98	0.02	υ_{asym} NH_2 (100)
2	3310w		3575	3425	29.25	254.12	0.09	υ_{sym} NH_2 (100)
3	3203m	3200vw	3203	3068	3.88	121.50	0.07	υ CH (97)
4	3079vw	3062m	3198	3064	6.89	202.80	0.11	υ CH (94)
5	3056vw		3193	3059	7.92	75.93	0.04	υ CH (97)
6			3184	3050	18.96	122.69	0.07	υ CH (99)
7			3178	3045	12.22	128.05	0.07	υ CH (97)
8			3177	3043	14.89	66.93	0.04	υ CH (99)
9			3174	3041	7.59	134.81	0.08	υ CH (99)
10			3163	3031	0.08	48.51	0.03	υ CH (95)
11	3027vw		3157	3025	10.51	96.86	0.06	υ CH (99)
12	1648vs	1647ms	1711	1639	181.45	174.02	0.77	υ C═O (85)
13			1662	1634	155.47	20.17	0.10	ρ NH_2 (82)
14			1639	1611	17.38	68.54	0.34	υ CC_{ring} (60) + ρ NH_2 (10)
15			1636	1608	55.17	145.71	0.73	υ CC_{ring} (68)
16	1597s	1599s	1619	1592	29.48	41.78	0.22	υ CC_{ring} (80)
17	1577s		1616	1588	7.59	7.60	0.04	υ CC_{ring} (81)
18			1520	1495	9.87	0.56	0.00	β CH (34) + υ CC_{ring} (17)
19	1486vs	1489vw	1518	1492	14.37	5.15	0.03	β CH (50) + υ CC_{ring} (24)
20	1456s	1459vw	1481	1456	74.48	6.02	0.04	υ CC_{ring} (40) + β CH (25)
21	1445w	1447vw	1475	1450	7.98	4.35	0.03	β CH (53) + υ CC_{ring} (30)
22			1356	1333	16.56	2.37	0.02	υ CC_{ring} (71) + β CH (25)
23	1325w	1326w	1352	1329	10.29	1.07	0.01	β CH (69) + υ CC_{ring} (22)
24			1339	1316	115.52	11.55	0.10	β CH (43) + υ CC_{ring} (13) + υ CN (12)
25			1333	1311	14.36	0.78	0.01	υ CC_{ring} (64) + β CH (13)
26	1289w	1289vw	1309	1287	178.37	29.75	0.27	β CH (31) + υ CN (19) + υ $C_{12}C_{13}$ (19)
27	1253w	1264vw	1263	1242	129.97	33.41	0.34	υ_{asym} $C_2C_{12}C_{13}$ (29) + υ CN (14)
28	1180w	1181w	1201	1181	16.77	2.47	0.03	β CH (72) + υ CC_{ring} (15)
29			1193	1173	2.10	3.22	0.04	β CH (72) + υ CC_{ring} (16)
30		1160w	1183	1163	0.23	4.65	0.06	β CH (75) + υ CC_{ring} (17)
31	1135vw	1135w	1154	1135	16.90	30.76	0.39	β CH (30) + υ CC_{ring} (19) + υ_{sym} $C_2C_{12}C_{13}$ (17)
32			1129	1109	1.10	18.16	0.24	υ CC_{ring} (30) + β CH (25) + r NH_2 (23)
33		1083vw	1103	1084	5.56	0.34	0.01	υ CC_{ring} (44) + β CH (39)
34	1075vw		1086	1067	1.96	1.29	0.02	υ CC_{ring} (35) + r NH_2 (37) + β CH (10)
35	1028vw	1031w	1049	1031	2.90	18.03	0.29	υ CC_{ring} (47) + β CH (12)
36	1001vw	1002s	1017	999	2.07	57.62	1.00	Ring 1 deformation (71)
37	995ms		1011	994	1.42	6.76	0.12	Ring 2 deformation (57)
38			1009	992	1.54	4.61	0.08	γ CH (68)
39	985w	986vw	998	981	25.64	46.33	0.84	υ CC_{ring} (28)
40			995	978	0.76	8.18	0.15	γ CH (68)
41			980	963	0.75	0.85	0.02	γ CH (84)
42	929m	933w	952	936	1.94	0.74	0.02	γ CH (83)
43	898w	901vw	909	894	6.41	0.79	0.02	γ CH (77)
44	884w		895	880	10.72	0.65	0.02	γ CH (89)
45	846w	851w	863	849	1.44	1.99	0.05	γ CH (99)
46			856	841	54.28	5.33	0.14	υ CC_{ring} (23) + υ CN (13) + β CCO (12)
47	805w	808w	820	806	6.60	0.73	0.02	γ CCC (40)
48	776w	779vw	792	778	24.36	0.95	0.03	γ CH (61)
49	724w	726vw	737	724	65.35	9.71	0.36	γ CH (44)
50	708w	710vw	719	707	34.15	13.00	0.51	β CCC (19) + υ_{sym} $C_2C_{12}C_{13}$ (12)
51	693vs		708	696	17.72	0.73	0.03	γ CH (76)
52	686s		694	682	6.81	0.53	0.02	γ CCC (66)
53	643m	643vw	658	647	30.30	1.73	0.08	β CCC (29) + β CCO (18)
54		620vw	632	621	0.20	5.37	0.29	Ring 1 deformation (79)
55	597w	596vw	609	598	6.76	10.99	0.64	β $C_2C_{12}C_{13}$ (16)
56	538vw	539vw	546	537	151.04	4.02	0.30	ω NH_2 (53)
57	518vw	518vw	543	534	6.93	4.59	0.34	ring 2 def. (32) + υ CN (12)
58			507	498	196.37	5.48	0.48	ω NH_2 (44) + γ CCC (11)
59	449vw		455	447	2.10	0.11	0.01	γ CCC (55) + r NH_2 (10)
60	434vw		440	432	4.00	0.62	0.07	γ CCC (63)
61	406vw	409vw	416	409	0.71	1.63	0.22	γ CCC (94)
62		385vw	397	391	0.23	1.29	0.19	r NH_2 (54)
63			376	369	6.38	0.57	0.10	β CCO (33) + υ_{asym} $C_2C_{12}C_{13}$ (17)
64		274vw	304	299	17.25	0.53	0.14	t NH_2 (99)
65		255vw	267	262	1.11	1.67	0.01	υ_{sym} $C_2C_{12}C_{13}$ (29) + β CCC_{12} (21)

Table 3 (*Continued*)

Mode nos.	Experimental wavenumbers (cm^{-1})			Theoretical wavenumbers (cm^{-1}) B3LYP/6-311++G(d,p)				Vibrational assignments with TED (≥10%)
	FT-IR	FT-Raman	Unscaled	Scaled	I_{IR}[a]	SA_{Ra}[b]	I_{Ra}[c]	
66			237	233	2.48	3.98	0.02	γ NH_2 (33) + γ CCC (30) + γ CCC_{12} (12)
67		210w	208	204	2.35	0.98	0.01	β CCC_{12} (41) + γ CCC (18)
68			192	189	2.47	4.40	0.03	β CCC_{12} (32) + γ CCC (25)
69		152ms	134	132	0.84	1.48	0.01	γ CCC (53) + γ C=O (40)
70		105vs	89	88	0.41	5.26	0.08	γ rings (79)
71			56	55	0.81	6.45	0.15	γ rings (80)
72			33	33	2.52	1.08	0.04	γ rings (93)

w – weak, vw – very weak, s – strong, vs – very strong, m – medium, ms – medium strong.

[a] I_{IR} – IR intensity (K $mmol^{-1}$).

[b] SA_{Ra} – Raman scattering activity ($Å^4$/amu).

[c] I_{Ra} – Raman intensity (Arb. units) (relative Raman intensities and normalized to 1, TED < 10% are not shown), ν – stretching; β – in-plane-bending; γ – out-of-plane bending; ρ – scissoring; ω – wagging; r – rocking; t – twisting.

show very good agreement with our experimental work; the bands observed in the range 1325–1028 cm^{-1} in FT-IR spectrum and 1326–1031 cm^{-1} in FT-Raman. The out of plane bending frequencies of the C—H bonds on the aromatic ring are in the region of 950–600 cm^{-1}. The intensities of these vibrations are usually medium or strong [31]. The frequencies of these modes depend mainly on the number of the adjacent hydrogen atoms on the ring and are not significantly affected by the nature of the substituents. Moreover, the substitution patterns on the ring can be judged from the out of plane bending of the C—H bonds, which appear in the region 900–675 cm^{-1} [32]. In our present study, the C—H out-of-plane bending vibrations are calculated in the region 992–696 cm^{-1} and are well coherence with the experimental data. It can be found that the frequencies increase with decrease of the number of adjacent hydrogen atoms in the benzene ring.

5.3.2. Amino group vibrations

The methylene and amino groups are generally referred to as electron donating substituents in aromatic ring system [33]. The CH_2 interacts with nearby π-systems via hyperconjugation, while the NH_2 share its lone pair of electrons with the π-electrons in a ring. Both mechanisms imply electronic delocalization is taken into account by the molecular orbital approach. The NH_2 group gives rise to six internal modes of vibrations such as the asymmetric stretching (υ_{as}), symmetric stretching (υ_s), the symmetric planar deformation or scissoring (ρ_s), the antisymmetric planar deformation or rocking (r_{as}), the symmetric non-planar deformation or wagging (ω) and the anti-symmetric non-planar deformation or torsion (τ). The molecule under investigation possesses one NH_2 group and hence one can expect one asymmetric and one symmetric N—H stretching vibrations. It is stated that in amines, the N—H stretching vibrations occur in the region 3500–3300 cm^{-1}. The asymmetric —NH_2 stretching vibration appears from 3500 to 3420 cm^{-1} and the symmetric —NH_2 stretching is observed in the range 3420–3340 cm^{-1}. The antisymmetric (υ_{as}) stretching mode is calculated at the higher wavenumber 3520 cm^{-1} than the symmetric (υ_s) one at 3425 cm^{-1} by B3LYP/6-311++G(d,p) method having mode nos. 1 and 2 as seen in Table 3. The infrared spectrum of title molecule shows a medium band observed at 3389 cm^{-1} corresponding to NH_2 asymmetric stretching mode. The symmetric stretching also observed as weak band in IR spectrum at 3310 cm^{-1}.

The scissoring mode of the NH_2 group appears in the region 1615–1650 cm^{-1} in benzene derivatives with NH_2 substituents. The calculated frequency for the scissoring mode of NH_2 is 1634 and 1611 cm^{-1} (mode nos. 13 and 14) for 3-ABP. This mode (mode no. 14) is also coupled with ring stretching mode as shown in Table 3. The rocking mode of the NH_2 group appears in the range 1000–1100 cm^{-1} with variable IR intensity [33]. The observed weak band at 1075 cm^{-1} in IR spectrum is attributed to the appreciable contribution from the C—H in plane bending suggests its origin due to the rocking mode. It is a strongly mixed mode containing contribution from the planar C—H deformation and the rocking mode. The theoretically predicted frequency by B3LYP method at 233 cm^{-1} is assigned to NH_2 out-of-plane bending vibration.

5.3.3. C—C and C=O vibrations

Most of the ring vibrational modes are affected by the substitutions in the ring of the title molecule. The characteristic ring stretching vibrations are assigned in the region 1650–1300 cm^{-1} [34,35]. Most of the computed frequencies by B3LYP/6-311++G(d,p) method are assigned for C=C and C—C stretching vibrations almost coincides with experimental data without scaling. The (C=C) vibrations are more interesting if the double bonds are in conjugation with the ring. The presence of conjugate substituents such as C=O, C=C, C=N or the presence of heavy element causes a doublet formation. Therefore, the C—C stretching vibrations of 3-ABP are found in the range 1597–1325 cm^{-1} in IR and 1599–1326 cm^{-1} in Raman spectrum. The theoretically computed values for C—C vibrational modes by B3LYP/6-311++G(d,p) method give excellent agreement with experimental data. The calculated CCC in-plane bending and out-of-plane bending vibrations are also in good agreement with the experimental data. The ring out-of-plane bending vibrations are calculated at low wavenumbers with maximum TED contribution.

The interaction of carbonyl group with other groups present in the system did not produce such a drastic and characteristic changes in the frequency of C=O stretch as did by interaction of N—H stretch. The carbon–oxygen double bond is formed by p_π–p_π between carbon and oxygen. Because of the different electronegativities of carbon and oxygen atoms, the bonding electrons are not equally distributed between the two atoms. The lone pair of electrons on oxygen also determines the nature of the carbonyl group. The position of the C=O stretching vibration is very sensitive to various factors such as the physical state, electronic effects by substituents, ring strains [36]. Normally carbonyl group vibrations occur in the region 1850–1600 cm^{-1} [37]. In this study, the C=O stretching vibration of 3-ABP is observed at 1648 cm^{-1} in the FT-IR and 1647 cm^{-1} in the FT-Raman spectrum, and this mode is confirmed by their TED value of 85%. The calculated frequency is well correlated with the experimental data. The in-plane and out-of-plane bending vibrations of C=O group have also been identified and presented in Table 3.

5.4. Electronic absorption spectra

The energies of four important molecular orbitals of 3-ABP: the second highest and the highest occupied MO's (HOMO and

Table 4
Experimental and computed absorption wavelength λ (nm), excitation energies *E* (eV) and oscillator strengths (*f*) of 3-aminobenzophenone in ethanol, gas phase, chloroform and DMSO solutions.

Experimental TD-DFT/6-311 + +G(d,p)										
Ethanol		Gas			Chloroform			DMSO		
E (eV)	λ (nm)	*E* (eV)	λ (nm)	(*f*)	*E* (eV)	λ (nm)	(*f*)	*E* (eV)	λ (nm)	(*f*)
		3.4727	357.03	0.0254	3.3295	372.38	0.0399	3.2809	377.89	0.0399
3.6513	340	3.6125	343.21	0.0058	3.7007	335.03	0.0041	3.7438	331.18	0.0038
5.0671	245	4.5877	270.25	0.0112	4.5079	275.04	0.0149	4.4741	277.12	0.0147

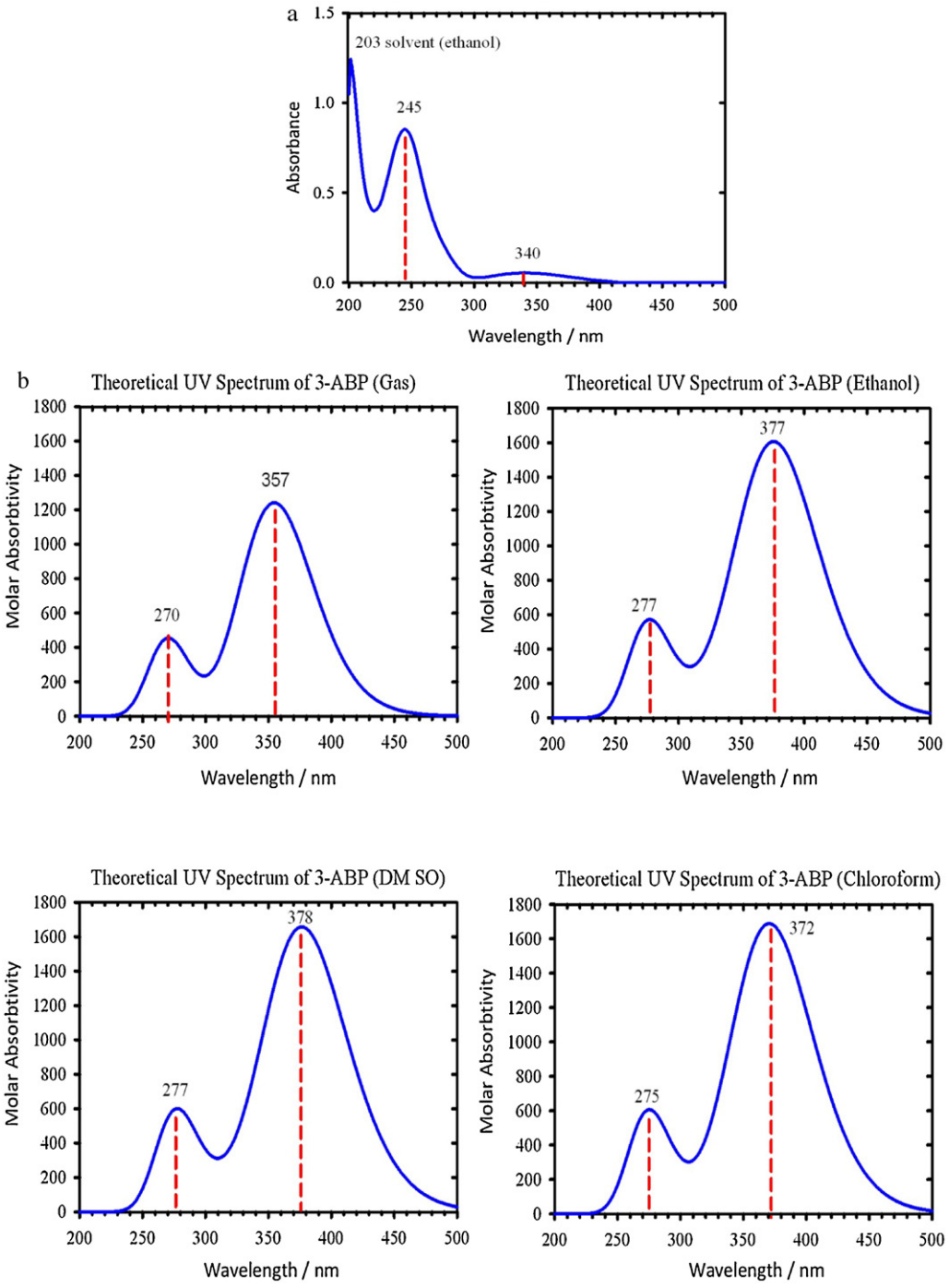

Fig. 4. (a) Experimental (ethanol) UV spectrum of 3-ABP and (b) theoretical UV spectra of 3-ABP.

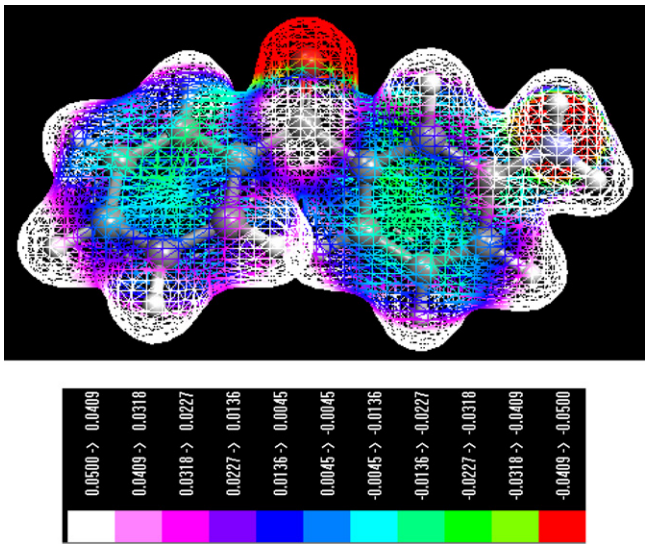

Fig. 5. Molecular electrostatic potential map calculated at B3LYP/6-311++G(d,p) level.

HOMO−1), the lowest and the second lowest unoccupied MO's (LUMO and LUMO+1) were calculated. The lowest singlet → singlet spin-allowed excited states of 3-ABP were taken into account for the TD-DFT calculation in order to investigate the properties of electronic absorption. The experimental λ_{max} values are obtained from the UV/visible spectrum recorded in ethanol. The calculations were also performed with gas phase, $CHCl_3$ and DMSO solvent. The calculated absorption wavelengths (λ_{max}) and the experimental wavelengths are also given in Table 4. The experimental and theoretical absorption spectra are shown in Fig. 4 (a) and (b). In the electronic absorption spectrum of 3-ABP, there are three absorption bands with a maximum 340 nm, 245 nm and 203 nm (solvent). The predicted absorption wavelength is at 357.03, 343.21, 270.25 nm in gas phase, 372.38, 335.03, 275.04 nm in chloroform and 377.89, 331.18, 277.12 nm in DMSO solution. It is obvious that to use TD-DFT calculations to predict the electronic absorption spectra is a quite reasonable method. The dipole moment in a molecule is another important electronic property that results from non-uniform distribution of charges on the various atoms in a molecule. It is mainly used to study the intermolecular interactions involving the van der Waals type dipole–dipole forces, etc., because the larger the dipole moment, stronger will be the intermolecular interactions [38]. The calculated dipole moment values for the molecules are also given in Table 5.

5.5. Molecular electrostatic potential (MEP) analysis

The molecular electrostatic potential, $V(r)$, at a given point r (x, y, z) in the vicinity of a molecule, is defined in terms of the interaction energy between the electrical charge generated from the molecule electrons and nuclei and a positive test charge (a proton) located at r. The molecular electrostatic potential (MEP) is related to the electronic density and is a very useful descriptor for determining sites for electrophilic attack and nucleophilic reactions as well as hydrogen-bonding interactions [39,40]. To predict reactive sites for electrophilic and nucleophilic attack for the title molecule, MEP was calculated at the B3LYP/6-311++G(d,p) optimized geometry. The negative (red) regions of MEP were related to electrophilic reactivity and the positive (white) regions to nucleophilic reactivity shown in Fig. 5. The negative regions are mainly localized on the carbonyl oxygen atom, O23 atom. Also, a negative electrostatic potential region is observed around the nitrogen atom (N24 atom). A maximum positive region is localized on the hydrogen atoms indicating a possible site for nucleophilic attack. The MEP map shows that the negative potential sites are on electronegative atoms as well as the positive potential sites are around the hydrogen atoms. These sites give information about the region from where the compound can have noncovalent interactions.

5.6. First order hyperpolarizability and Frontier molecular orbital analysis

The first hyperpolarizability (β_0) of this molecular system, and related properties (β, α_0 and $\Delta\alpha$) of 3-ABP are calculated using B3LYP/6-311++G(d,p) method, based on the finite-field approach. In the presence of an applied electric field, the energy of a system is a function of the electric field. First order hyperpolarizability is a third rank tensor that can be described by $3 \times 3 \times 3$ matrices. The 27 components of the 3D matrix can be reduced to 10 components due to the Kleinman symmetry [41]. It can be given in the lower tetrahedral format. It is obvious that the lower part of the $3 \times 3 \times 3$ matrices is a tetrahedral. The components of β are defined as the coefficients in the Taylor series expansion of the energy in the external electric field. When the external electric field is weak and homogeneous, this expansion becomes:

$$E = E^0 - \mu_\alpha F_\alpha - \tfrac{1}{2}\alpha_{\alpha\beta}F_\alpha F_\beta - \tfrac{1}{6}\beta_{\alpha\beta\gamma}F_\alpha F_\beta F_\gamma + \cdots$$

where E^0 is the energy of the unperturbed molecule, F_α is the field at the origin, μ_α, $\alpha_{\alpha\beta}$ and $\beta_{\alpha\beta\gamma}$ are the components of dipole moment, polarizability and the first order hyperpolarizabilities, respectively. The total static dipole moment μ, the mean polarizability α_0, the anisotropy of the polarizability $\Delta\alpha$ and the mean first hyperpolarizability β_0, using the x, y, z components they are defined as:

$$\mu = (\mu_x^2 + \mu_y^2 + \mu_z^2)^{1/2}$$

$$\alpha_0 = \frac{\alpha_{xx} + \alpha_{yy} + \alpha_{zz}}{3}$$

$$\alpha = 2^{-1/2}[(\alpha_{xx} - \alpha_{yy})^2 + (\alpha_{yy} - \alpha_{zz})^2 + (\alpha_{zz} - \alpha_{xx})^2 + 6\alpha_{xx}^2]^{1/2}$$

$$\beta_0 = (\beta_x^2 + \beta_y^2 + b_z^2)^{1/2}$$

and

$$\beta_x = \beta_{xxx} + \beta_{xyy} + \beta_{xzz}$$

$$\beta_y = \beta_{yyy} + \beta_{xxy} + \beta_{yzz}$$

$$\beta_z = \beta_{zzz} + \beta_{xxy} + \beta_{yyz}$$

Since the values of the polarizabilities (α) and hyperpolarizability (β) of the Gaussian 03 output are reported in atomic units (a.u.), the calculated values have been converted into electrostatic units (esu) (α: 1 a.u. = 0.1482×10^{-24} esu; β: 1 a.u. = 8.639×10^{-33} esu).

The total molecular dipole moment and first hyperpolarizability are 3.4485 Debye and 5.6041×10^{-30} esu, respectively and are depicted in Table 2. Total dipole moment of title molecule is approximately two times greater than those of urea and first hyperpolarizability of title molecule is 15 times greater than those of urea (μ and β of urea are 1.3732 Debye and 0.3728×10^{-30} esu obtained by HF/6-311G(d,p) method).

To understand this phenomenon in the context of molecular orbital theory, we examined the molecular HOMOs and molecular LUMOs of the title compound. When we see the first hyperpolarizability value, there is an inverse relationship between first hyperpolarizability and HOMO–LUMO gap, allowing the molecular orbitals to overlap to have a proper electronic communication

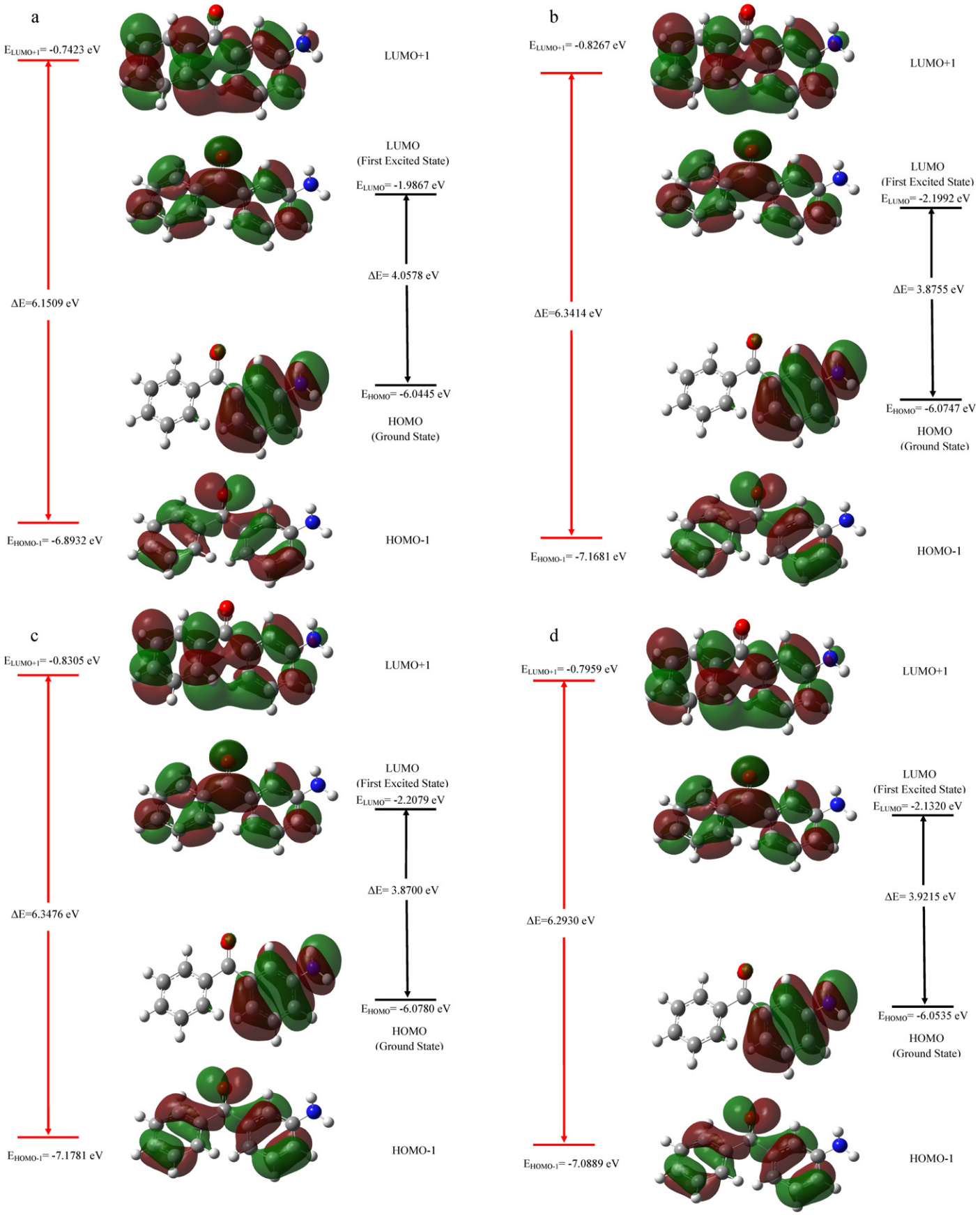

Fig. 6. (a) The frontier and second frontier molecular orbitals of 3-ABP in gas phase. (b) The frontier and second frontier molecular orbitals of 3-ABP in ethanol solution. (c) The frontier and second frontier molecular orbitals of 3-ABP in DMSO solution. (d) The frontier and second frontier molecular orbitals of 3-ABP in chloroform solution.

Table 5
Calculated energy (eV) and dipole moment (Debye) values of 3-aminobenzophenone in gas phase, ethanol, chloroform and DMSO solutions.

	Gas	Ethanol	Chloroform	DMSO
E_{total} (Hartree)	−632.15916	−632.17083	−632.16759	−632.17125
E_{HOMO} (eV)	−6.0445	−6.0747	−6.0535	−6.0780
E_{LUMO} (eV)	−1.9867	−2.1992	−2.1320	−2.2079
ΔE_{HOMO}–E_{LUMO} gap (eV)	4.0578	3.8755	3.9215	3.8700
E_{HOMO-1} (eV)	−6.8932	−7.1681	−7.0889	−7.1781
E_{LUMO+1} (eV)	−0.7423	−0.8267	−0.7959	−0.8305
ΔE_{HOMO-1}–E_{LUMO+1} gap (eV)	6.1509	6.3414	6.2930	6.3476
Dipole moment	3.4485	4.7379	4.3340	4.7931

conjugation, which is a marker of the intramolecular charge transfer from the electron donating group through the π-conjugation system to the electron accepting group [42,43].

Many organic molecules, containing conjugated π-electrons characterized by large values of molecular first hyperpolarizabilities were analyzed by means of vibrational spectroscopy [44,45]. In most cases, even in the absence of inversion symmetry, the strongest bands in the Raman spectrum are weak in the IR spectrum and vice versa. But the intramolecular charge transfer from the donor to accepter group through a single–double bond conjugated path can induce large variations of both the molecular dipole moment and the molecular polarizability, making IR and Raman activity strong at the same time. The most important orbitals in a molecule are the frontier molecular orbitals, called HOMO and LUMO. These orbitals determine the way the molecule interacts with other species. The frontier orbital gap helps to characterize the chemical reactivity and kinetic stability of the molecule. A molecule with a small frontier orbital gap is more polarizable and is generally associated with a high chemical reactivity, low kinetic stability and is also termed as soft molecule [46]. The frontier molecular orbitals play an important role in the electric and optical properties, as well as in UV–vis spectra and chemical reactions [47,48]. The conjugated molecules are characterized by a small highest occupied molecular orbital–lowest unoccupied molecular orbital (HOMO–LUMO) separation, which is the result of a significant degree of intramolecular charge transfer from the end-capping electron-donor groups to the efficient electron-acceptor groups through π-conjugated path [49].

The HOMO represents the ability to donate an electron, LUMO as an electron acceptor represents the ability to obtain an electron. The HOMO and LUMO energy calculated by B3LYP/6-311++G(d,p) method is shown below. This electronic absorption corresponds to the transition from the ground to the first excited state and is mainly described by one electron excitation from the HOMO to the LUMO. While the energy of the HOMO is directly related to the ionization potential, LUMO energy is directly related to the electron affinity. Energy difference between HOMO and LUMO orbital is called as energy gap that is an important stability for structures [50] and is given in Table 5. The plots of highest occupied molecular orbitals (HOMOs) and lowest unoccupied molecular orbitals (LUMOs) are shown in Fig. 6 (a-d).

HOMO is located over the amino group and ring 2; the HOMO → LUMO transition implies an electron density transfer to benzene ring 1 from amino group and ring 2 through the carbonyl group. Moreover, these orbital significantly overlap in their position for 3-ABP and lower in the HOMO and LUMO energy gap explains the eventual charge transfer interactions taking place within the molecule.

$$\text{HOMO energy (B3LYP)} = -6.0445\,\text{eV}$$

$$\text{LUMO energy (B3LYP)} = -1.9867\,\text{eV}$$

$$\text{HOMO–LUMO energy gap (B3LYP)} = -4.0578\,\text{eV}$$

6. Conclusions

The detailed interpretation of the vibrational spectra of 3-aminobenzophenone has been carried out with the aid of scaled quantum mechanical force field methodology. FT-IR and FT-Raman spectra of the 3-aminobenzophenone have been recorded and analyzed. The molecular geometry, vibrational wavenumbers, UV–vis spectral analysis, HOMO and LUMO energy of 3-aminobenzophenone in the ground state have been calculated by using density functional theory. The geometrical structure shows a little distortion due to the substitution of carbonyl group and amino group. The observed and the calculated wavenumbers are found to be in good agreement. The UV spectrum was measured in ethanol solution and compared with theoretical values in gas phase, chloroform and DMSO environment (PCM model) using TD-DFT/B3LYP/6-311++G(d,p) basis set. The lowering of the HOMO–LUMO energy gap value has substantial influence on the intramolecular charge transfer of the molecule. The 3-ABP molecule is highly conjugated and π electron delocalized.

References

[1] S. Genbo, G. Shouwu, P. Feng, H. Youping, L. Zhengdong, J. Phys. D: Appl. Phys. 26 (1993) B236–B237.
[2] V.I. Pavlovskii, O.V. Kulikov, T.L. Karaseva, Ukr. Khim. Zh. 64 (1998) 123–128.
[3] S.A. Andronati, S. Yu Makan, Ukr. Khim. Zh. 65 (1999) 5–17.
[4] A. Mamo, S. Nicoletti, N.C. Tai, Molecules 7 (2002) 618–627.
[5] J.I. Ubeda, M. Vilacampa, C. Avendano, Synthesis 8 (1999) 1335–1340.
[6] S.A. Andronati, V.I. Pavlovskii, O.V. Kulikov, Y.A. Simonov, M. Gdanets, J. Struct. Chem. 42 (2001) 871–876.
[7] E.A. Fehnel, J. Org. Chem. 32 (1996) 2899–2902.
[8] I.H. Sternbach, Angew. Chem. Int. Ed. Engl. 10 (1971) 34–43.
[9] S. Herrero, M.T. Garcia-Lopez, R. Herranz, J. Org. Chem. 68 (2003) 4582–4585.
[10] X.H. Duan, X.Y. Li, R.X. He, X.M. Cheng, J. Chem. Phys. 122 (2005) 084314 (1–9).
[11] X.M. Cheng, Y. Huang, J.Y. Ma, X.Y. Li, Chin. J. Chem. Phys. 20 (2007) 273–278.
[12] P. Sett, T. Misra, S. Chattopadhyay, A.K. De, P.K. Mallick, Vib. Spectrosc. 44 (2007) 331–342.
[13] M. Tsonkov Kolev, A. Bistra Stamboliyska, Spectrochim. Acta 56A (1999) 119–126.
[14] L.X. Hong, G.X. Yang, Z.X. Zhou, Comp. Theor. Chem. 976 (2011) 191–196.
[15] Gaussian Inc., Gaussian 03 Program, Gaussian Inc., Wallingford, 2004.
[16] J. Zhang, H.M. Xiao, J. Chem. Phys. 116 (2002) 10674–10678.
[17] X.J. Xu, H.M. Xiao, X.H. Ju, X.D. Gong, W.H. Zhu, J. Phys. Chem. 110A (2006) 5929–5933.
[18] Z.X. Chen, J.M. Xiao, H.M. Xiao, Y.N. Chiu, J. Phys. Chem. 103A (1999) 8062–8066.
[19] A.D. Becke, J. Chem. Phys. 98 (1993) 5648–5652.
[20] C. Lee, W. Yang, R.G. Parr, Phys. Rev. B37 (1988) 785–789.
[21] J.P. Perdew, Y. Wang, Phys. Rev. B33 (1986) 8800–8802.
[22] A. Frisch, A.B. Nielsen, A.J. Holder, Gauss View Users Manual, Gaussian Inc., Pittsburgh, PA, 2000.
[23] SQM version 1.0, Scaled Quantum Mechanical Force Field, 2013 Green Acres Road, Fayetteville, Arkansas 72703.
[24] G. Keresztury, S. Holly, J. Varga, G. Besenyei, A.Y. Wang, J.R. Durig, Spectrochim. Acta 49A (1993) 2007–2026.
[25] G. Keresztury, in: J.M. Chalmers, P.R. Griffith (Eds.), Raman Spectroscopy: Theory, in Handbook of Vibrational Spectroscopy, vol. 1, John Wiley & Sons Ltd, New York, 2002.
[26] R. Dennington II, T. Keith, J. Millam, Gauss View, Version 4.1.2, Semichem, Inc., Shawnee Mission, KS, 2007.
[27] M.D. Halls, J. Velkovski, H.B. Schlegel, Theor. Chem. Acc. 105 (2001) 413–421.
[28] J. Coates, in: R.A. Meyers (Ed.), Interpretation of Infrared Spectra: A Practical Approach, John Wiley and Sons Ltd., Chichester, 2000.
[29] H. Spedding, D.H. Whiffen, Proc. Roy. Soc. Lond. A 238 (1956) 245–255.

[30] M. Silverstein, G.C. Basseler, C. Morill, Spectrometric Identification of Organic Compounds, Wiley, New York, 1981.
[31] I.F. Shishkov, N.I. Sadova, V.P. Novikov, L.V. Vikov, Zh. Strukt. Khim. 25 (1984) 98–102.
[32] P.S. Kalsi, Spectroscopy of Organic Compounds, Wiley Eastern Limited, New Delhi, 1993, p. 116.
[33] N.B. Colthup, L.H. Daly, S.E. Wiberley, Introduction to Infrared and Raman Spectroscopy, Academic Press, New York, 1990.
[34] J. Tonannavar, J. Yenagi, V.B. Veenasangeeta Sortur, M.V. Jadhav, Kulkarni, Spectrochim. Acta A 77 (2010) 351–358.
[35] G. Socrates, Infrared and Raman Characteristic Group Frequencies – Tables and Charts, third ed., Wiley, Chichester, 2001.
[36] D.N. Sathyanarayana, Vibrational Spectroscopy, Theory and Applications, New Age International Publishers, New Delhi, 2004.
[37] R.L. Prasad, A. Kushwaha, M. Suchita, R.A. Kumar, Y. Yadav, Spectrochim. Acta A 69 (2008) 304–311.
[38] D.P. Chemica, Scholar Res. Libr. 2 (2010) 48–58.
[39] E. Scrocco, J. Tomasi, Adv. Quantum Chem. (1979) 11–115.
[40] N. Okulik, A.H. Jubert, Internet Electron J. Mol. Des. (2005) 4–17.
[41] D.A. Kleinman, Phys. Rev. 126 (1962) 1977–1979.
[42] M.C. Ruiz Delgado, V. Hernandez, J. Casado, J.T. Lopez Navarre, J.M. Raimundo, P. Blanchard, J. Roncali, J. Mol. Struct. 151 (2003) 651.
[43] J.P. Abraham, D. Sajan, V. Shettigar, S.M. Dharmaprakash, I. Nemec, I.H. Joe, V.S. Jayakumar, J. Mol. Struct. 917 (2009) 27.
[44] T. Vijayakumar, I. Hubert Joe, C.P.R. Nair, V.S. Jayakumar, Chem. Phys. 343 (2008) 83–99.
[45] M.A. Palafox, Int. J. Quantum Chem. 77 (2000) 661–684.
[46] I. Fleming, Frontier Orbitals and Organic Chemical Reactions, John Wiley and Sons, New York, 1976.
[47] Fleming, Frontier Orbitals, Organic Chemical Reactions, Wiley, London, 1976.
[48] T. Karakurt, M. Dinçer, A. Çetin, M. Sekerci, Spectchim. Acta 77A (2010) 189–198.
[49] C.H. Choi, M. Kertesz, J. Phys. Chem. A 101 (1997) 3823–3831.
[50] D.F.V. Lewis, C. Ioannides, D.V. Parke, Xenobiotica 24 (1994) 401–408.